UNCLASSIFIED

AERE - M 2159

1

AERE - M 2159

AD A953138

United Kingdom Atomic Energy Authority

RESEARCH GROUP

Memorandum

AD A953138

STUDIES OF TWO-PHASE FLOW PATTERNS BY SIMULTANEOUS X-RAY AND FLASH PHOTOGRAPHY

G. F. HEWITT D. N. ROBERTS

DTIC FILE COPY

DTIC
ELECTE
NOV 1 1984
D

Chemical Engineering Division,

Atomic Energy Research Establishment,

Harwell, Berkshire.

1969

Available from H. M. Stationery Office

© - UNITED KINGDOM ATOMIC ENERGY AUTHORITY - 1969
Enquiries about copyright and reproduction should be addressed to the Scientific Administration Office, Atomic Energy Research Establishment, Harwell, Didcot, Berkshire, England.

U.D.C.
532.529
778.37

1. Introduction

In the study of two-phase, gas-liquid flow, it is often useful to distinguish between a number of possible interface configurations or "flow patterns" or "flow regimes". Such delineation has the potential of leading to a much more adequate symmetrical description of the flow and also allows the engineer to obtain a much better qualitative picture of what is happening in the piece of equipment with which he is concerned, for example, in steam generating plant.

The most common method of identifying the flow pattern is to use visual observation. Where necessary, this can be extended by use of both still and cine photography. By using high speed cine techniques, patterns which appear as formless blurs to the eye, can be seen to have well established characteristics. Examples of the increasing use of high speed photography are given, for instance, by Cooper, Hewitt and Pinchin[1], Brown and Govier[2] and Arnold and Hewitt[3]. Unfortunately, however, the use of visible light for the photography of two-phase flow has a serious limitation. The signal received by the camera is a result of a complex set of refractions and reflections from the interfaces present in the flow. Often, the complexity of the signal is such that it is quite impossible to infer anything meaningful from it.

A natural extension of visible light photography is the use of X-rays. Preliminary experiments on the use of X-rays are reported by Derbyshire, Hewitt and Nicholls[4] who used a medical X-ray unit to photograph air-water flow. In spite of the relatively long exposures which this equipment gave, it was possible to take satisfactory pictures of a number of flow patterns.

Studies of flow patterns in high pressure steam-water mixtures are reported by Bennett, Hewitt, Kearsey, Keeys and Lacey[5] who used both visual and X-ray techniques. Most of the results were obtained from assessment of high speed cine films backed up by a limited number of flash X-ray photographs and also some preliminary results from the investigations reported in this present memorandum. Bennett et al defined the following flow patterns:

(1) Bubble flow In bubble flow, the gas is moving as isolated bubbles in a liquid continuum.

(2) Slug flow In slug flow, bubbles which have nearly the same diameter as the tube and which have a characteristic rounded front, move along the tube separated by liquid slugs which may or may not contain a dispersion of smaller bubbles.

(3) Churn flow As the gas velocity is increased (i.e. by increasing the heat flux and therefore the outlet steam quality) the slug flow regime begins to break down and the gas bubbles are unstable. In large diameter tubes, this instability leads to an oscillating, "churning" flow. This oscillatory type of behaviour is much less marked in small diameter tubes but a region of instability of the gas bubbles is still present and it is convenient to use the name "churn flow" to cover this region; alternative names might be "semi-annular" or "unstable slug".

(4) Wispy annular flow In this regime, there is a continuous, relatively slow-moving, liquid film on the tube walls and a more rapidly moving entrained phase in the core of the channel. This description also fits annular flow (see below) but the "wispy

annular" regime is characterised by the nature of the entrained phase. This phase appeared to flow in large agglomerates somewhat resembling ectoplasm. Also in this region, the liquid film itself tends to entrain gas bubbles.

(5) Annular flow In annular flow, there is a liquid film on the wall with a continuous gas core in the centre of the channel. The gas core can contain entrained droplets, but Bennett et al drew a distinction between the condition where the entrained liquid is agglomerated (i.e. in "wispy annular flow") and where the entrained phase is broken up into small droplets. Clearly the distinction between "wispy" annular and "ordinary" annular must be somewhat subjective, but it is worth attempting to distinguish between the two regimes. The flow pattern diagram obtained by Bennett et al drew a distinction between the condition where the entrained liquid is agglomerated (i.e. in "wispy annular flow") and where the entrained phase is broken up into small droplets. Clearly the distinction between "wispy" annular and "ordinary" annular must be somewhat subjective, but it is worth attempting to distinguish between the two regimes. The flow pattern diagram obtained by Bennett et al for steam-water flow in a 0.5 inch bore tube at 1000 psia is reproduced in Figure 1.

In taking X-ray photographs for high pressure flow, Bennett et al[5] were in some difficulty in finding a material which would withstand the high pressures and yet be sufficiently transparent to X-rays to allow a reasonable distinction to be made between the two phases. Although this problem was partially solved by the use of a specially designed titanium tube, considerable sacrifices had to be made of definition. It was impossible to study the fine structure of the flows; however, the results were still useful in providing a general support to the direct visual observations.

The present experiments were designed to supplement the high pressure visualisation experiments. The most important objective was to obtain high-definition X-ray photographs of two-phase flow at high liquid flowrates. This region is of very great technological importance and one in which the flow pattern is extremely difficult to distinguish by visible light observation. Some studies in this region are reported by Chaudry, Emerton and Jackson[6]. These authors show a large zone of unidentifiable flow pattern in the high liquid rate region. Their results provide a further illustration of the need for better visualisation techniques.

In designing the present experiments, the volumetric flows were selected so as to cover a range of parameters of interest in the SGHWR. In this respect, the investigation is somewhat limited and no attempt was made to make a comprehensive study over the whole range of parameters possible. Nevertheless, some 128 separate X-ray photographs have been obtained with widely varying flow conditions.

2. Experimental

2.1 Rig circuit and test section

The experiments were carried out on the LOTUS (LOng TUbe System), a full description of which will be published shortly. Briefly, the loop consists of a system for circulating air and water through a vertical tube of total length 77 ft. Air is taken from the site mains, filtered and metered and is fed to the bottom of the tube. It then passes through a calming length before meeting the water stream which

is injected through an injector around the periphery of the tube. For the lower water flowrates, the injector consisted of a porous wall section, but at the highest water flowrates used, the porous sinter was removed since it gave unacceptable pressure loss. The water was circulated from a separation tank, via a two-stage vortex centrifugal pump to the liquid injector. The two-phase mixture was separated on leaving the test section tube and the water recirculated, the air being rejected to atmosphere.

In the present experiments, the air entered the tube and passes through a 7 ft long calming section before meeting the water stream. A further 33 ft 9 in of tube were allowed for the establishment of flow pattern before the flow passes through the viewing section (see below). Pressure tappings were inserted at positions just above the liquid injector and just below the viewing section.

2.2 Visualisation techniques

The viewing section consisted of a 1 ft long Perspex block which could be inserted between flanges of the 1.25 inch bore tube sections. The block was bored to give a continuous wall of the same diameter as the tube and its outer cross section was 2 inch square. The use of square outer walls has been shown to give better visualisation using visible light[1].

The X-ray film was attached to one side of the block and the X-ray beam entered from the opposite side. The source - manufactured by the Field Emission Corporation* - gave pulses of duration of the order 10^{-7} seconds. The energy of the pulses was approximately 100 kV; the exposure time was sufficiently short to resolve practically all of the phenomena of interest in the present context and was comparable with the fastest available light source.

The X-ray source was positioned at 15 inches from the viewing block and an approximately 10 inch long field of view was covered. For the X-radiography, a relatively fine grain film (typically Kodak Industrex D) was employed as a recording medium. The film was mounted in a cassette and was placed behind a standard salt screen.

A still camera was placed so as to give a field of view at right angles to that seen by the X-ray source. For illumination, a special purpose spark source was used operating at 8 kV giving a spark duration of about 0.2 microseconds with an energy of approximately 12 joules. The spark source was placed on the opposite side of the tube to the camera. The positioning of the various units is illustrated in Figure 2. The visible light photographs were recorded on Polaroid Land film, type 57 (3,000 ASA) with an aperture of f.11. The shutter of the camera was opened just before the exposure was made and to prevent stray light entering the camera between the period between the opening of the shutter and the spark discharge, a light proof temporary structure was brought around the viewing area as illustrated in Figure 2. The spark discharge and X-ray discharge were triggered simultaneously by use of a special 30 volt trigger circuit.

*The proprietary names of equipment and materials are given in this memorandum so that readers can appreciate the type of equipment, etc. used. It is not to imply that similar equipment or materials by other manufacturers would be less satisfactory.

DTIC COPY INSPECTED 3

3. Results and Discussion

Full details of the experiments together with the original photographs and X-ray film are stored in the Archives of AERE, Harwell. Table 1 gives a list of the experiments and shows the various flow and pressure conditions which were used. The fluid temperature was of the order of 70°F during these experiments.

The individual photographic records from each test were examined and the following classification evolved:

(A) Bubble flow. In this regime, a dispersion of bubbles occurs in a liquid continuum. Photographs and radiographs illustrating this regime are shown in Figures 3 and 4 for very low and relatively high gas flowrates respectively.

(B) Bubble flow with large gas bubbles of the plug flow type. This regime falls within the definition of plug flow given in the introduction and is illustrated in Figures 5 and 6 respectively. The visible light and X-ray records are inter-located by means of a wire which was placed on the tube wall and can be seen in both records.

(C) Annular flow with a bubbly film, but with no sign of wisps in the gas core. An example of this kind of result is given in Figure 7.

(D) Annular flow with a bubble-free film. This regime occurs at relatively low liquid flowrates and is illustrated in Figure 8. On the visible light photographs, a disturbance wave can be seen though this is not easily apparent on the print of the radiograph.

(E) Annular flow with evidence of the core liquid agglomeration (wispy annular flow). This type of flow is well illustrated by Figures 9 and 10.

(X) In some cases of an essentially bubble type flow, some evidence of the development of larger gas occlusions can be seen without these occlusions taking the characteristic form associated with plug flow. An example of this type of situation is given in Figure 11.

(Y) Liquid film flow with bubble entrainment in the liquid film and evidence of large waves on the surface. By comparison with other studies, this regime can be identified as being associated with churn flow and examples of the results obtained in this region are given in Figures 12 and 13.

In considering the photographic and interpretative evidence given in this memorandum, the reader should bear in mind the following important points:

(1) Much more information can be gained from studying the actual X-ray film than is visible from the prints from it.

(2) An essential limitation of still photography is that, by its very nature, it can only record the instantaneous distribution of the phases at a point. The existence of flow patterns implies that this distribution will change continuously with time. For example, in plug flow, if a large gas bubble passes the point of observation at the time of the exposure, then the regime may appear, superficially, to be annular flow.

(3) It was not possible, on economic grounds, to obtain sufficient information in the present studies to allow a thorough statistical analysis.

The identification of the various exposures on the above classification is given in Table 1. The results are also plotted in terms of superficial phase velocities in Figure 14.

It is desirable to achieve direct comparability between the present tests and those carried out in high pressure steam-water systems. To achieve this, it is necessary to find some suitable scaling parameter. A preliminary examination of the results showed that the flow pattern transitions occurred at very different superficial phase velocities for the two cases and a simple scaling on the basis of phase velocity does not appear to fit. Numerous methods of scaling of flow patterns have been proposed in the literature. The most widely used flow pattern chart is that of Baker[7] who studied flow patterns in horizontal pipelines and plotted the flow pattern observations in terms of the parameters (G_G/λ) and $(G_L\lambda\psi/G_G)$ where G_G and G_L are the superficial mass velocities of the gas and liquid phases respectively. The parameters λ and ψ are functions of the physical properties of the fluids and are defined by the following equations, which scale the values of the parameters to give unity for both λ and ψ for atmospheric pressure and temperature in air-water mixtures:

$$\lambda = [(\rho_G/0.075)(\rho_L/62.3)]^{\frac{1}{2}} \qquad \text{..... (1)}$$

$$\psi = (73/\sigma) \; [\mu_L \; (62.3/\rho_L)^2]^{1/3} \qquad \text{..... (2)}$$

In the above equations, ρ_G and ρ_L are the densities of the gas and liquid phases respectively, σ the surface tension and μ_L the liquid viscosity. An examination of the above correlation shows that the first parameter is proportional to $(\rho_G^{\frac{1}{2}} V_G) \; \rho_L^{-\frac{1}{2}}$ and the second parameter is proportional to $(\rho_L^{1/3} V_L/\rho_G V_G)$ for given surface tension and viscosity. Here, V_G and V_L are the gas and liquid superficial velocities respectively. The Baker correlation is thus seen to contain, in the first parameter, the grouping $(\rho_G^{\frac{1}{2}} V_G)$ which is the square root of the superficial momentum flux of the gas phase. Wallis[8] has suggested the use of the following parameters in evaluating transitions from one regime to another:

$$V_G^* = V_G \; \rho_G^{\frac{1}{2}} \; [gD \; (\rho_L - \rho_G)]^{-\frac{1}{2}} \qquad \text{..... (3)}$$

$$V_L^* = V_L \; \rho_L^{\frac{1}{2}} \; [gD \; (\rho_L - \rho_G)]^{-\frac{1}{2}} \qquad \text{..... (4)}$$

where D is the tube diameter and g is the acceleration due to gravity. It has been suggested that the "flow reversal transition" - which may correspond approximately with the transition from churn to annular flow - occurs at a value of V_G^* of 0.7 - 1. Again, it will be noted that the group V_G^* contains the square root of the superficial momentum flux.

The above discussion illustrates the disparity of scaling factors which have been used though a common factor of superficial momentum flux appears to be apparent.

The present data were plotted in terms of the parameters $\rho_G \; V_G^2$ and $\rho_L \; V_L^2$, the superficial momentum fluxes of the gas and liquid phases respectively, as shown in Figure 15. The data for steam-water flow at pressures of 500 and 1000 psia respectively are plotted on the same co-ordinates in Figure 16. In spite of the smaller values of diameter, surface tension and viscosity for the steam-water case, an approximately consistent

flow pattern map can be derived based on the present air-water data and the steam-water data of reference 5, when the data are plotted in this manner. It should be emphasized from the outset that this flow pattern map should be regarded as a first approximation; clearly, very much more extensive data would be needed before any definite conclusions could be drawn. It is most unlikely that the simple parameters of momentum flux will describe the flow patterns in widely differing fluids to any degree of accuracy. Clearly, the physical properties of the fluids and the characteristics of the channel would have to be taken into account. However, in comparing the present data with the steam-water data from reference 5, there seems to be no justification for using a more complicated form of plotting.

In Figures 15 and 16, flow pattern types were designated as follows:

(1) Plug flow: the method of injection of the fluids in the present tests would tend to favour the formation of plug flow and, in any case, this type of flow would be expected to develop rapidly from bubble flow due to bubble coalescence.

(2) Churn flow: the lower boundary of this region is somewhat uncertain. The upper boundary is also somewhat uncertain but is drawn in as indicated based on the data for the steam-water system. On Figure 15, the values of $\rho_G V_G^2$ corresponding to $V_G^* = 1$ are given for the air-water and steam-water systems respectively. For the steam-water flow, the transition into an annular type flow is predicted reasonably well by using this value (as was noted in reference 5) but the air-water system does not appear to fit under the conditions of high water flowrate studied in the present experiments. Hewitt, Lacey and Nicholls[9] found that the flow reversal transition occurred at $V_G^* = 0.7 - 0.9$ but the maximum liquid flowrate studied was somewhat lower than the minimum in the present tests. Furthermore, the transition from churn to annular flow would be expected to occur at somewhat lower values of gas velocity than does the flow reversal transition; the complex relationship between the two transitions is discussed in detail in reference 9.

(3) Annular flow: in reference 5, it was suggested that the transition from annular to wispy annular flow occurred at a constant liquid velocity. A closer look at the data obtained from the present investigations and from the steam-water tests, indicates that, at higher gas flowrates, the transition line may move over to higher liquid flowrates as indicated in Figures 15 and 16. This seems to be reasonable since the liquid agglomerates would tend to break up as the gas velocity is increased.

(4) Wispy annular flow: the present photographs give a direct confirmation of the existence of liquid agglomerates in the gas core of an annular-type flow. Usually, in this region, the liquid film is rather thick and contains a dispersion of gas bubbles. Gas bubble entrainment in the liquid film can also occur in the churn flow regime as shown in Figure 15.

(5) Bubble flow with developing structure: at high liquid flowrates, there are strong indications from the present experiments that the bubble flow regime may be more stable than the plug flow regime. Thus, the turbulence in the flow may be sufficient to break up bubbles and thus prevent the formation of the large cylindrical bubbles characteristic of plug flow. However, as the gas flowrate is increased in this region,

the formation of irregular shaped gas voids occurs and ultimately leads to the onset of wispy annular flow. There is thus a direct, though gradual, transition from a bubble type flow to an annular type flow. In a boiling channel, where the gas velocity increases as a result of evaporation, this gradual transition will occur along the channel.

4. Conclusions

The use of high speed flash photography coupled with simultaneous X-radiography has proved a powerful technique in the evaluation of the detailed structure of two-phase flows. This technique has proved particularly valuable in the region of high liquid mass flows where an evaluation of structure and flow pattern is particularly difficult.

On the basis of the present data, obtained with an air-water system, and on previous data obtained with steam-water flow, it has been possible to draw a tentative flow pattern map in terms of the parameters $\rho_G V_G^2$ and $\rho_L V_L^2$. The regimes of plug, churn, annular and wispy annular flow were identified and in the last named regime it was shown that liquid agglomerates did in fact exist in the gas core. At high liquid flowrates there appeared to be a gradual transition from bubble flow to wispy annular flow without the intermediate stage characteristic of plug flow.

Although the present data have provided some relevant information on the structure of two-phase flows, it should be emphasized that they are somewhat limited in scope. There seems to be a good case for extending the technique to cover a much wider range of parameters in much greater detail.

Acknowledgements

The authors wish to acknowledge the assistance given to them in the experimental work by Mr. L. E. Gill and by Mr. R. T. P. Derbyshire (who assisted with the X-ray photography).

References

1. Cooper, K.D., Hewitt, G.F. and Pinchin, B. "Photography of two-phase gas-liquid flow". J.Photo.Sci., 12, 269, (1964). (See also AERE - R 4301, (1963)).

2. Brown, R.A.S. and Govier, G.W. "High speed photography in the study of two-phase flow". Can.J.Chem.Eng., 39, 159, (1961).

3. Arnold, C.R. and Hewitt, G.F. "Further developments in the photography of two-phase gas-liquid flow". J.Photo.Sci., 15, 97, (1967).

4. Derbyshire, R.T.P., Hewitt, G.F. and Nicholls, B. "X-radiography of two-phase gas-liquid flow". AERE - M 1321, (1964).

5. Bennett, A.W., Hewitt, G.F., Kearsey, H.A., Keeys, R.K.F. and Lacey, P.M.C. "Flow visualisation studies of boiling at high pressure". Proc.Inst.Mech.Eng., 180, (Part 3c), 260, (1965-1966). (See also AERE - R 5874, (1965)).

6. Chaudry, A.B., Emerton, A.C. and Jackson, R. "Flow regimes in the co-current upwards flow of water and air". Symposium on Two Phase Flow, Exeter, June 1965, (Paper B2).

7. Baker, O. "Simultaneous flow of oil and gas". Oil & Gas Journal, 53, (12), 185, (July 1954).

8. Wallis, G.B. "The transition from flooding to co-current annular flow in a vertical tube". AEEW - R 142 (1962).

9. Hewitt, G.F., Lacey, P.M.C. and Nicholls, B. "Transitions in film flow in a vertical tube". Symposium on Two Phase Flow, Exeter, June 1965, (Paper B4). (See also AERE - R 4614, (1965)).

TABLE 1

Complete Experimental Data and Results of Photographic Examination

Run No.	W_L lb/hr	W_G lb/hr	Inlet Temps. Water °F	Inlet Temps. Air °F	Inlet Press psig	Pressure at Perspex Block psig	ρ_L at Block lb/ft^3	ρ_G at Block lb/ft^3	Air Superficial Velocity V_G ft/sec	Liquid Superficial Velocity V_L ft/sec	$\rho_L(V_L)^2$ lb/sec^2 ft	$\rho_G(V_G)^2$ lb/sec^2 ft	Regime (see Legend Below)
1	16050	112.4	74.5	75.0	59.5	42.5	62.08	0.28903	12.18	8.10	4073.1	42.88	C
2	15470	161.0	77.5	75.0	63.0	46.5	62.05	0.30925	16.31	7.81	3785.1	82.27	C
3	17200	226.6	75.0	72.0	77.5	58.5	62.08	0.37204	19.08	8.68	4677.3	135.4	E
4	16275	324.0	78.0	72.0	85.0	64.0	62.05	0.40000	25.37	8.22	4192.9	257.5	E
5	14250	422.0	77.0	72.0	85.0	64.0	62.06	0.40000	33.05	7.19	3208.5	436.9	C
6	18000	5.0	79.0	72.5	42.0	24.0	62.05	0.19688	0.80	9.09	5126.7	0.03	A
7	"	15.3	79.5	73.0	46.0	29.0	62.04	0.22157	2.16	9.09	5125.9	1.03	A
8	"	21.7	79.5	73.0	47.0	30.0	62.04	0.22663	3.00	9.09	5125.9	2.04	B
9	"	26.3	79.5	73.0	48.0	31.0	62.04	0.23170	3.56	9.09	5125.9	2.94	A
10	"	30.4	79.5	73.0	48.0	31.0	62.04	0.23170	4.11	9.09	5125.9	3.91	A
11	"	37.1	79.5	73.0	49.5	33.0	62.04	0.24185	4.81	9.09	5125.9	5.60	A
12	14300	422.0	79.5	73.0	85.0	64.0	62.04	0.39902	33.10	7.22	3233.8	437.2	C
13	18000	5.0	76.0	70.0	42.5	24.0	62.07	0.19754	0.79	9.08	5117.8	0.012	A
14	"	26.3	76.5	70.0	47.0	31.0	62.06	0.23326	3.53	9.09	5128.2	2.91	A
15	"	30.5	77.0	71.0	48.0	31.0	62.06	0.23226	4.11	9.09	5128.2	3.92	A
16	"	37.1	78.0	71.0	49.0	33.0	62.05	0.24243	4.79	9.09	5127.4	5.56	A
17	"	30.5	77.8	74.5	47.8	31.0	62.05	0.23092	4.14	9.09	5127.4	3.96	A
18	"	37.2	77.8	74.5	49.0	33.0	62.05	0.24103	4.84	9.09	5127.4	5.65	A
19	"	42.9	77.7	74.0	50.0	34.0	62.05	0.24608	5.46	9.09	5127.4	7.34	X
20	"	48.0	78.0	74.2	50.7	35.0	62.05	0.25114	5.99	9.09	5127.4	9.01	A
21	"	52.7	78.5	74.0	51.5	35.5	62.05	0.25367	6.51	9.09	5126.7	10.75	A
22	"	56.7	79.0	74.0	52.5	36.2	62.05	0.25367	7.00	9.09	5126.7	12.43	A
23	"	60.6	78.0	75.0	52.5	37.0	62.05	0.26125	7.27	9.09	5127.4	13.81	X
24	"	64.3	78.5	75.0	53.3	38.0	62.05	0.26630	7.56	9.09	5126.7	15.22	A
25	"	79.6	78.5	75.0	54.0	39.0	62.05	0.27135	9.19	9.09	5126.7	22.92	E
26	"	69.5	79.0	75.0	55.3	39.5	62.05	0.27388	7.95	9.09	5126.7	17.31	E
27	"	74.4	79.0	75.0	55.0	40.0	62.05	0.27641	8.43	9.09	5126.7	19.64	A
28	"	37.2	79.0	75.0	48.5	33.0	62.05	0.24103	4.84	9.09	5126.7	5.65	A
29	"	77.2	71.5	70.0	56.2	39.5	62.29	0.27547	8.78	9.06	5112.7	21.24	A
30	"	80.2	72.5	70.0	56.7	40.0	62.10	0.27801	9.04	9.08	5119.8	22.72	A
31	"	81.8	73.0	70.0	57.0	40.5	62.10	0.28055	9.13	9.08	5119.8	23.39	A
32	"	85.6	73.5	70.0	57.7	41.0	62.09	0.28309	9.47	9.08	5119.1	25.39	E
33	"	88.3	74.0	70.0	57.7	41.5	62.09	0.28563	9.68	9.08	5119.1	26.76	X
34	"	91.0	74.0	70.7	58.3	42.2	62.09	0.28825	9.89	9.08	5119.1	28.19	X
35	"	93.4	74.5	70.0	58.3	42.2	62.08	0.28825	10.15	9.08	5118.4	29.70	X
36	"	98.0	74.5	71.8	59.5	43.5	62.08	0.29580	10.38	9.08	5118.4	31.87	C
37	"	102.7	76.3	71.8	60.0	44.0	62.05	0.29834	10.78	9.09	5128.2	34.67	E
38	"	107.0	76.8	71.7	60.7	44.5	62.05	0.30088	11.14	9.09	5128.2	37.34	X
39	"	111.9	76.8	71.7	60.7	45.0	62.06	0.30342	11.55	9.09	5128.2	40.48	E
40	"	118.7	77.0	71.7	64.0	47.0	62.06	0.31359	11.86	9.09	5128.2	44.11	C
41	"	195.8	77.0	71.7	74.0	55.0	62.06	0.35425	17.31	9.09	5128.2	106.15	E
42	17125	270.5	77.0	71.7	82.5	63.0	62.06	0.39492	21.46	8.80	4806.2	181.87	E
43	9000	650.5	77.0	66.0	80.0	63.0	62.06	0.40034	50.90	4.54	1279.2	1037.20	E
44	9275	550.3	77.0	75.0	77.0	58.0	62.06	0.37140	46.41	4.68	1359.4	800.0	C
45	18000	5.0	78.0	70.0	43.0	25.0	62.05	0.20266	0.77	9.09	5127.4	0.12	A
46	600	1200.0	75.5	68.0	43.0	35.0	62.07	0.25456	147.70	0.303	56.99	5555.0	D
47	600	300.0	75.5	68.0	10.0	8.0	62.07	0.11627	80.82	0.303	56.99	759.0	D
48	18000	7.0	74.0	72.0	40.0	22.0	62.09	0.18415	1.19	9.08	5119.1	0.26	B
49	"	"	"	"	45.0	27.0	"	0.21213	1.03	"	"	0.23	B
50	"	"	"	"	50.0	34.0	"	0.24775	0.89	"	"	0.02	B
51	"	"	"	"	55.0	38.0	"	0.26809	0.82	"	"	0.018	B

TABLE 1 (Cont'd.)

Run No.	W_L lb/hr	W_G lb/hr	Inlet Temps. Water °F	Inlet Temps. Air °F	Inlet Press psig	Pressure at Perspex Block psig	ρ_L at Block lb/ft^3	ρ_G at Block lb/ft^3	Air Superficial Velocity V_G ft/sec	Liquid Superficial Velocity V_L ft/sec	$\rho_L (V_L)^2$ lb/sec^2 ft	$\rho_G (V_G)^2$ lb/sec^2 ft	Regime (see Legend Below)
52	18000	7.0	74.0	72.0	60.0	44.0	62.09	0.29862	0.73	9.08	5119.1	0.016	B
53	"	"	"	"	65.0	49.0	"	0.32405	0.68	"	"	0.015	B
54	"	"	"	"	70.0	54.0	"	0.34950	0.63	"	"	0.014	B
55	"	"	"	"	75.0	59.0	"	0.37493	0.59	"	"	0.013	A
56	"	"	"	"	80.0	64.0	"	0.40036	0.55	"	"	0.012	B
57	500	10.0	89.5	75.0	9.0	6.0	61.94	0.10461	2.99	0.253	39.65	0.94	C
58	"	20.0	"	"	11.0	6.5	"	0.10712	5.85	"	"	3.67	Y
59	"	30.0	"	"	12.0	9.0	"	0.11975	7.85	"	"	7.38	Y
60	"	40.0	"	"	14.0	10.0	"	0.12479	10.04	"	"	12.58	Y
61	"	50.0	90.2	72.0	17.0	13.0	"	0.14138	11.07	"	"	17.33	Y
62	"	60.0	"	75.0	19.0	16.0	"	0.15512	12.11	"	"	22.75	Y
63	"	70.0	"	75.0	23.0	19.0	"	0.17029	12.87	"	"	28.21	Y
64	"	80.0	90.5	72.0	28.0	25.3	"	0.20342	12.31	"	"	30.83	Y
65	"	90.0	90.2	75.0	27.0	"	"	0.20212	13.94	"	"	39.28	Y
66	"	100.0	"	"	26.0	"	"	"	15.40	"	"	47.93	Y
67	"	110.0	"	"	26.0	"	"	"	17.00	"	"	58.41	C
68	"	120.0	90.0	"	26.0	"	"	"	18.50	"	"	69.17	C
69	5000	10.0	83.0	"	36.0	"	62.01	"	1.54	2.53	396.9	0.48	E
70	"	20.0	83.0	"	36.0	"	62.01	"	3.09	2.53	"	1.93	A
71	"	30.0	82.0	"	36.0	"	62.02	"	4.64	2.53	"	4.35	A
72	"	40.0	79.0	77.5	35.0	"	62.05	0.20144	6.22	2.52	394.0	7.79	E
73	"	50.0	"	77.0	"	"	"	"	7.77	"	"	12.16	-
74	"	60.0	"	"	"	"	"	"	9.33	"	"	17.54	-
75	"	70.0	"	"	"	"	"	"	10.88	"	"	23.85	-
76	"	80.0	"	"	"	"	"	"	12.44	"	"	31.17	-
77	"	90.0	81.0	"	"	"	62.03	"	13.99	"	393.9	39.43	C
78	"	100.0	71.0	75.0	32.0	"	62.29	0.20209	15.50	2.51	392.5	48.55	C
79	"	110.0	"	75.6	"	"	"	"	17.05	"	"	58.75	C
80	"	120.0	"	75.0	"	"	"	"	18.60	"	"	69.92	E
81	15000	10.0	72.0	70.0	42.0	25.3	62.29	0.20431	1.53	7.54	3541.1	0.48	A
82	"	20.0	"	"	"	"	"	"	3.06	"	"	1.91	A
83	"	30.0	"	"	"	"	"	"	4.59	"	"	4.30	A
84	"	40.0	"	"	44.0	"	"	"	6.13	"	"	7.68	A
85	"	50.0	"	"	45.0	26.3	"	0.20939	7.48	"	"	11.72	X
86	"	60.0	"	"	46.5	27.8	"	0.21477	8.76	"	"	16.46	C
87	"	70.0	73.0	"	48.0	29.3	62.10	0.22464	9.76	7.57	3558.5	21.40	E
88	"	80.0	73.0	"	49.0	30.3	"	0.22972	10.90	7.57	3558.5	27.29	X
89	"	90.0	"	"	50.0	31.3	"	0.23481	12.00	"	"	33.8	X
90	"	100.0	"	"	52.0	33.3	"	0.24497	12.70	"	"	39.5	X
91	"	110.0	"	"	52.2	33.5	"	"	14.0	"	"	43.0	E
92	"	120.0	73.5	"	52.2	33.5	62.09	"	15.3	"	"	57.4	X
93	5000	10.0	72.0	71.0	57.0	45.3	62.29	0.30597	1.02	2.51	392.4	0.32	B
94	5000	20.0	"	"	60.0	"	"	"	2.04	"	"	1.27	A
95	"	30.0	"	"	58.0	"	"	"	3.07	"	"	2.88	B
96	"	40.0	"	"	55.0	"	"	"	4.09	"	"	5.12	X
97	"	50.0	"	"	"	"	"	"	5.11	"	"	7.99	X
98	"	60.0	"	"	"	"	"	"	6.14	"	"	11.5	Y
99	"	70.0	"	"	"	"	"	"	7.16	"	"	15.7	A
100	"	80.0	74.0	72.0	"	"	62.09	"	8.19	2.52	394.3	20.5	X

TABLE 1 (Cont'd.)

Run No.	W_L lb/hr	W_G lb/hr	Inlet Temps. Water °F	Inlet Temps. Air °F	Inlet Press psig	Pressure at Perspex Block psig	ρ_L at Block lb/ft^3	ρ_G at Block lb/ft^3	Air Superficial Velocity V_G ft/sec	Liquid Superficial Velocity V_l ft/sec	$\rho_L (V_L)^2$ lb/sec^2 ft	$\rho_G (V_G)^2$ lb/sec^2 ft	Regime (see Legend Below)
101	5000	90.0	74.0	72.0	55.0	45.3	62.09	0.30597	9.21	2.52	394.3	26.0	Y
102	"	100.0	72.0	"	"	"	62.29	"	10.2	2.51	392.4	31.8	Y
103	"	110.0	74.5	"	"	"	62.08	"	11.2	2.52	394.2	38.4	Y
104	"	120.0	75.0	"	"	"	"	"	12.2	2.52	"	45.5	Y
105	14000	10.0	"	"	"	"	"	"	1.02	7.06	3094.3	0.32	A
106	"	20.0	"	"	57.0	"	"	"	2.04	"	"	1.27	B
107	"	30.0	"	"	58.0	"	"	"	3.07	"	"	2.88	X
108	15000	40.0	"	"	60.0	"	"	"	4.09	7.57	3557.5	5.12	X
109	13350	50.0	"	"	62.0	"	"	"	5.11	6.74	2820.2	7.99	X
110	14000	60.0	"	"	61.0	46.0	"	0.30851	6.09	7.06	3094.3	11.4	X
111	14000	70.0	"	"	62.0	47.0	"	0.31359	6.99	7.06	"	15.3	X
112	13385	80.0	"	"	63.0	46.0	"	0.30851	8.12	6.75	2828.6	20.3	E
113	13475	90.0	70.5	68.0	60.0	45.3	62.29	0.30805	9.15	6.78	2863.5	25.8	A
114	13475	100.0	"	"	60.0	45.3	"	0.30805	10.1	"	"	31.4	E
115	13475	110.0	"	"	62.0	46.0	"	0.31061	11.0	"	"	37.6	A
116	13475	120.0	72.0	69.0	64.0	47.0	"	0.31573	11.9	"	2863.2	44.7	E

FLOW REGIMES LEGEND

A - Bubble

B - Bubble with plug

C - Annular with bubbly film

D - Annular with bubble free film

E - Annular with wisps and bubbly film

X - Evidence of structure

Y - Churn flow (bubbly liquid film)

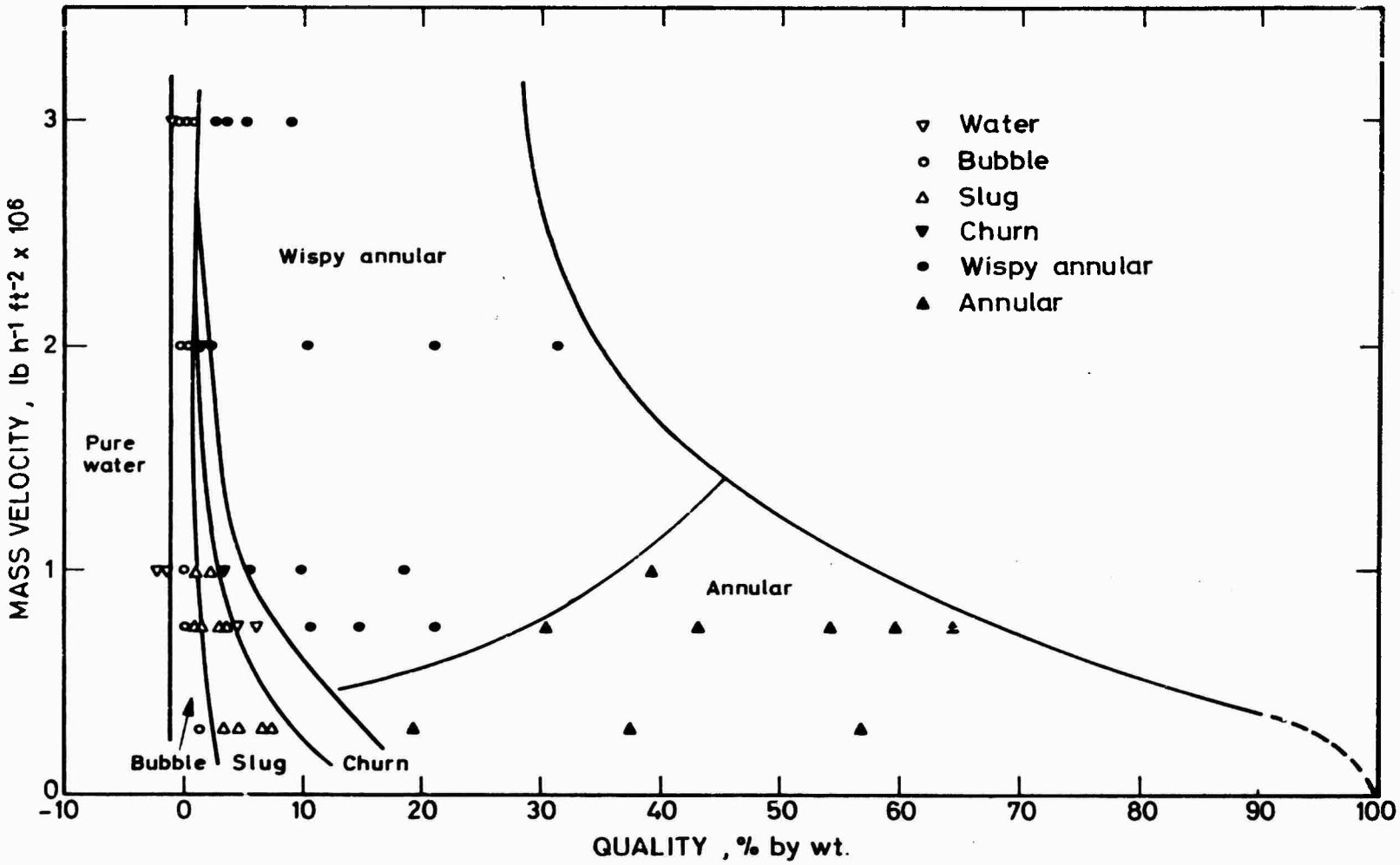

FLOW PATTERN DIAGRAM OBTAINED BY BENNETT ET AL[5] FOR STEAM-WATER FLOW IN A 0·5 INCH BORE TUBE AT 1000 lb/in².

FIGURE 1. A.E.R.E. M.2159

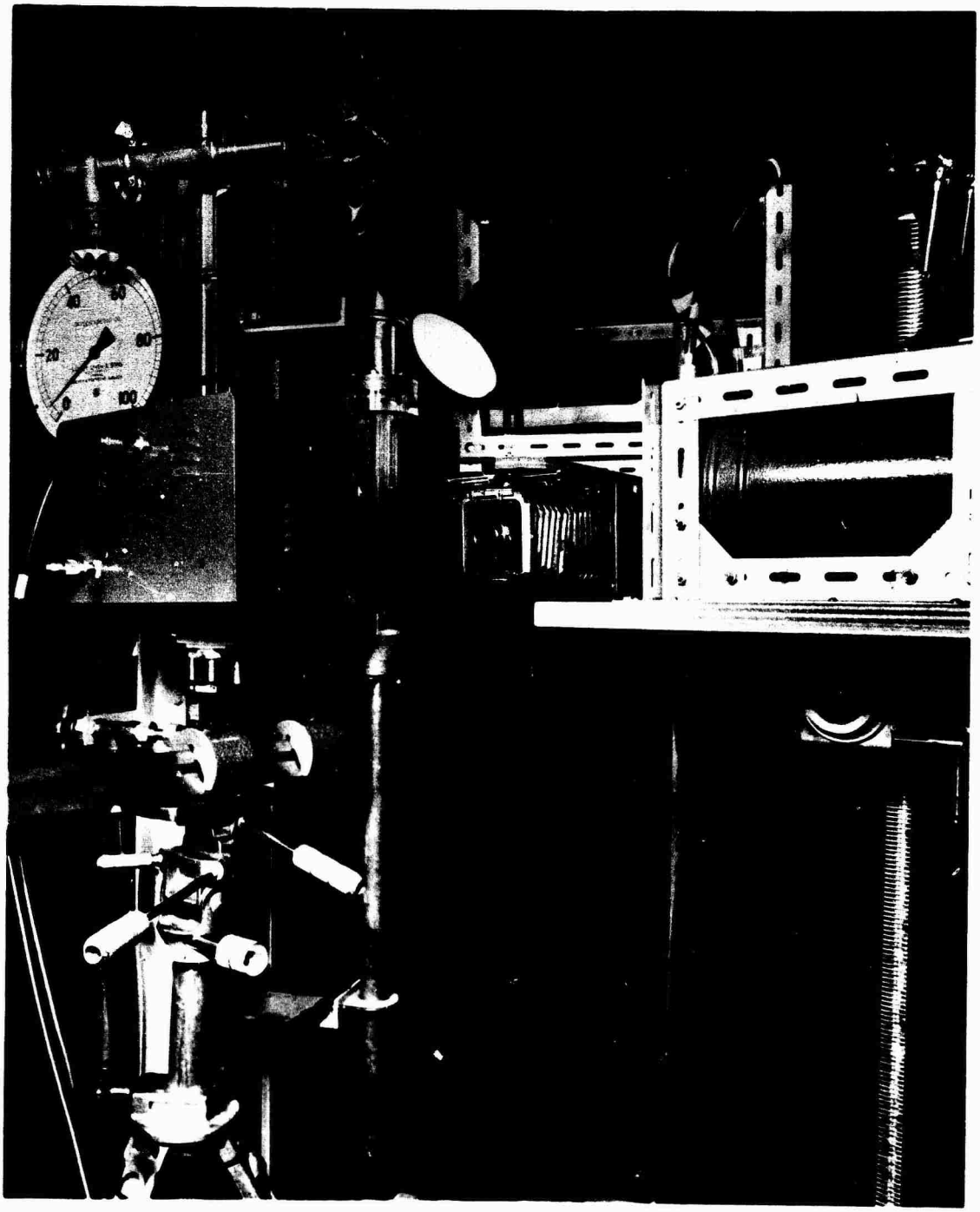

AERE - M 2159 Fig. 2

Positioning of X-ray source, camera and spark source with respect to viewing section.

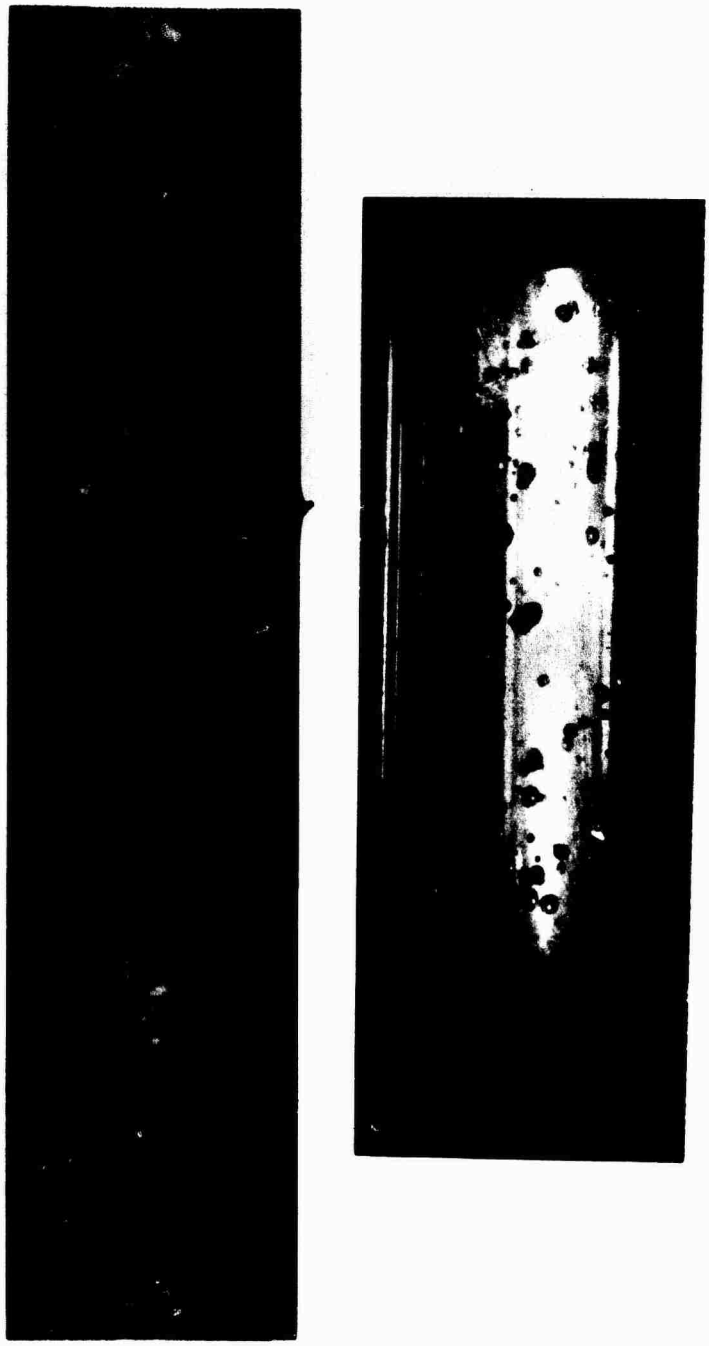

X-ray Flash

AERE - M 2159 Fig. 3

Simultaneous X-ray and flash photographs of air-water flow in the bubble regime.

Run No. 6

Pressure = 24.0 PSIG.

Superficial gas velocity (V_G) = 0.8 ft/sec.

Superficial liquid velocity (V_L) = 9.09 ft/sec.

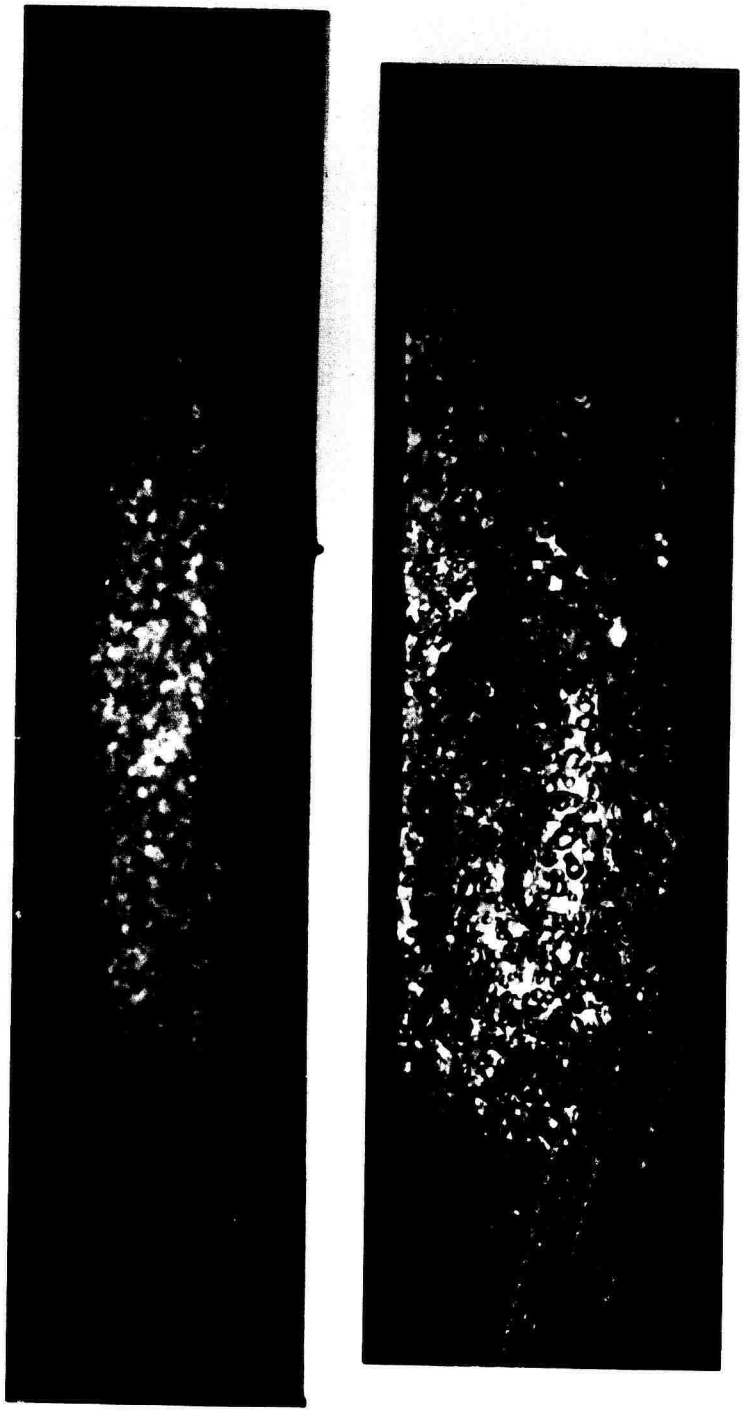

X-ray Flash

AERE - M 2159 Fig. 4

Simultaneous X-ray and flash photographs of air-water flow in the bubble regime.

Run No. 10

Pressure = 31.0 PSIG

Superficial gas velocity (V_G) = 4.11 ft/sec.

Superficial liquid velocity (V_L) = 9.09 ft/sec.

X-ray

Flash

AERE - M 2159 Fig. 5

Simultaneous X-ray and flash photographs of air-water flow in the plug regime.

Run No. 52

Pressure = 44.0 PSIG

Superficial gas velocity (V_G) = 0.73 ft/sec.

Superficial liquid velocity (V_L) = 9.08 ft/sec.

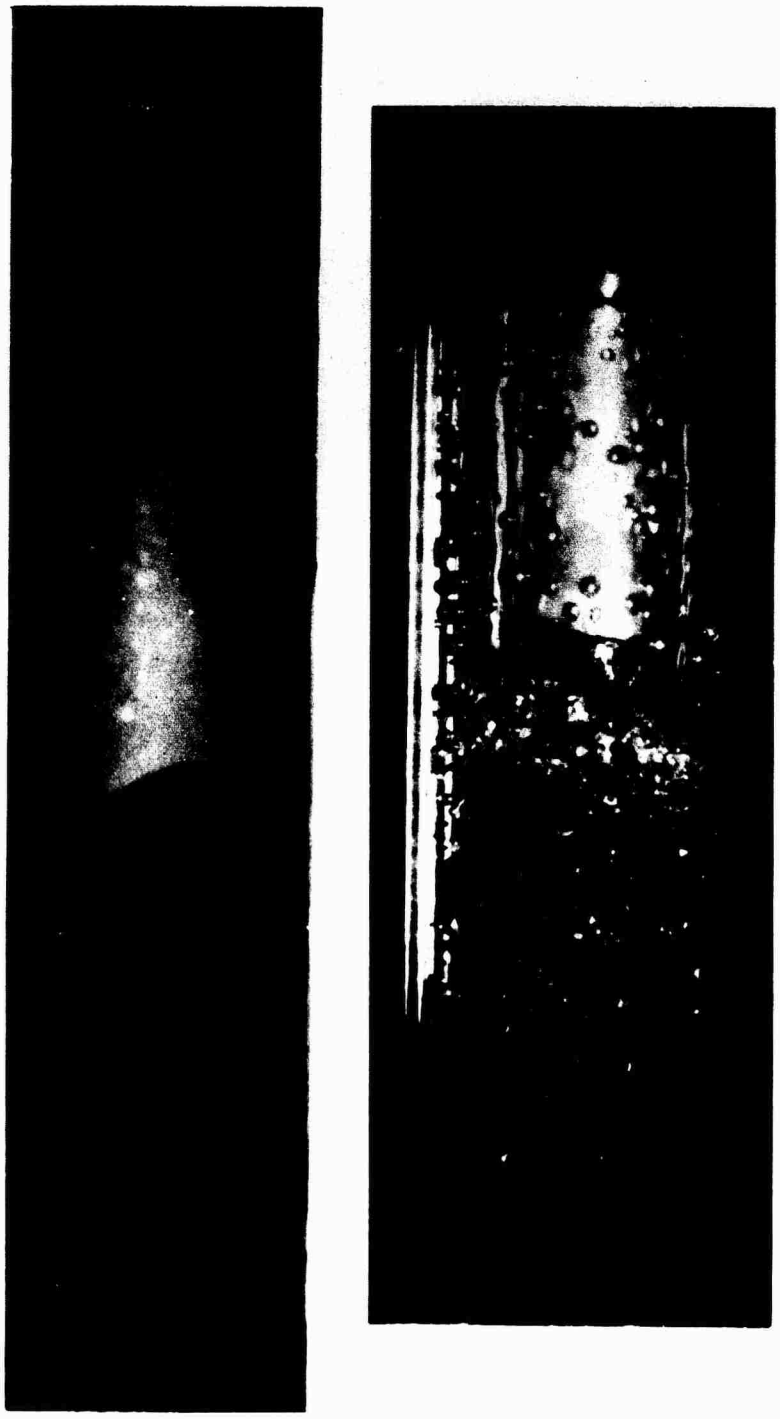

X-ray Flash

AERE - M 2159 Fig. 6

Simultaneous X-ray and flash photographs of air-water flow in the plug regime.

Run No. 93

Pressure = 45.3 PSIG

Superficial gas velocity (V_G) = 1.02 ft/sec.

Superficial liquid velocity (V_L) = 2.51 ft/sec.

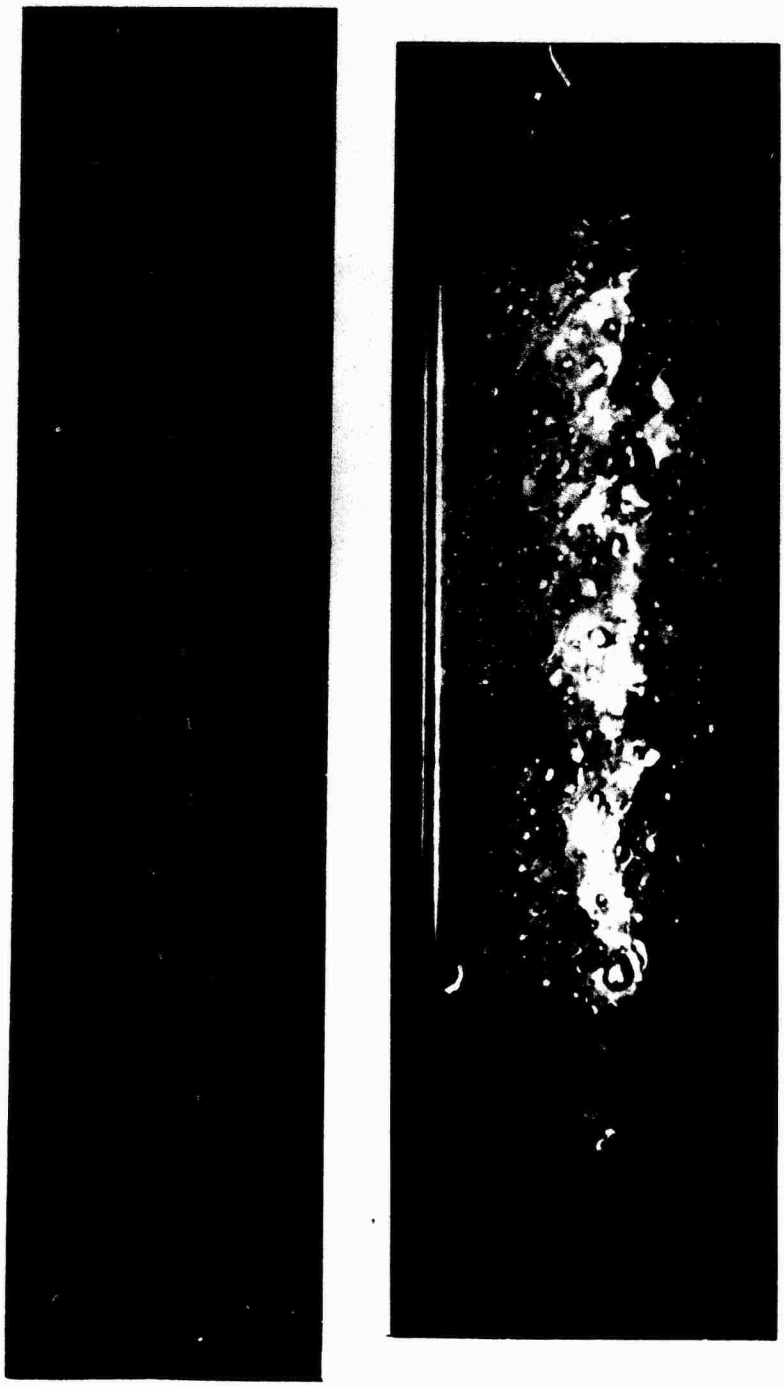

X-ray Flash

AERE - M 2159 Fig. 7

Simultaneous X-ray and flash photographs showing annular flow with a bubbly film.

Run No. 78

Pressure = 25.3 PSIG

Superficial gas velocity (V_G) = 15.5 ft/sec.

Superficial liquid velocity (V_L) = 2.51 ft/sec.

X-ray

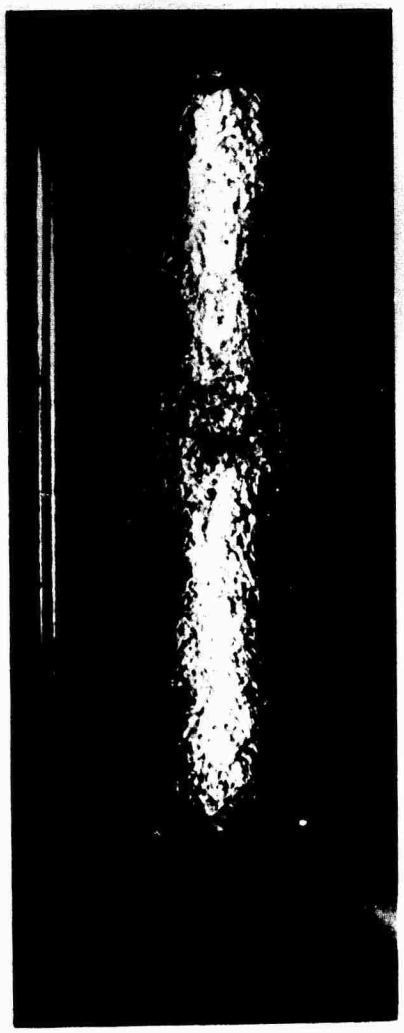

Flash

AERE - M 2159 Fig. 8

Simultaneous X-ray and flash photographs showing annular flow with a bubble-free film.

Run No. 46

Pressure = 35.0 PSIG

Superficial gas velocity (V_G) = 147.7 ft/sec.

Superficial liquid velocity (V_L) = 0.303 ft/sec.

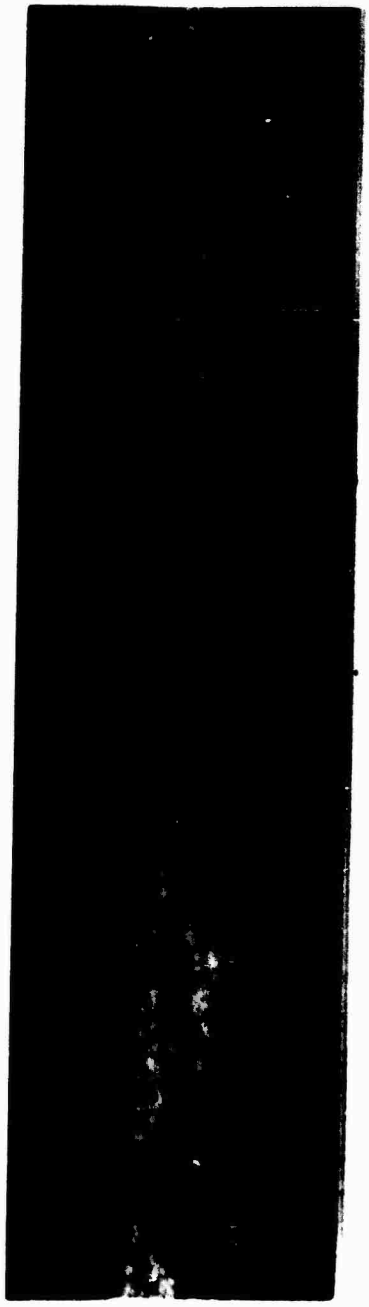

X-ray

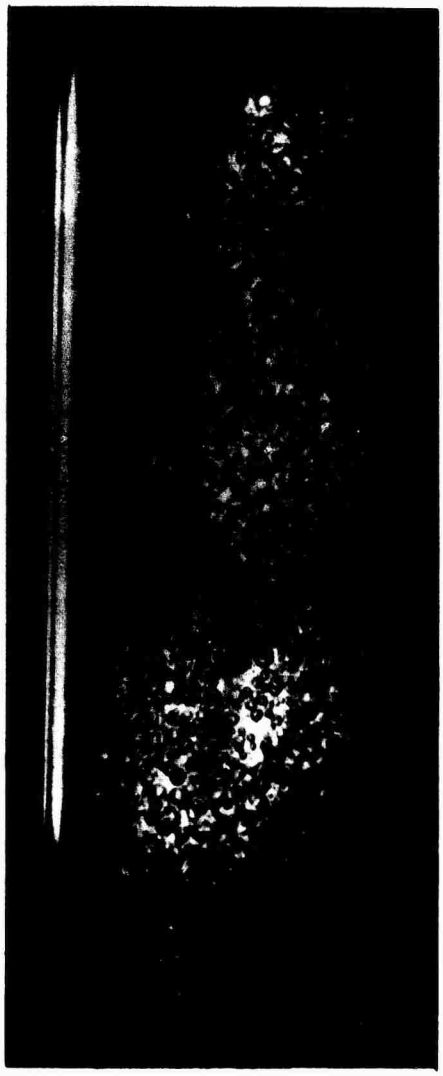

Flash

AERE - M 2159 Fig. 9

Simultaneous X-ray and flash photographs of air-water flow in the wispy annular regime.

Run No. 39

Pressure = 45.0 PSIG

Superficial gas velocity (V_G) = 11.55 ft/sec.

Superficial liquid velocity (V_L) = 9.09 ft/sec.

X-ray Flash

AERE - M 2159 Fig. 10

Simultaneous X-ray and flash photographs of air-water flow in the wispy annular regime.

Run No. 35

Pressure = 42.2 PSIG

Superficial gas velocity (V_G) = 10.15 ft/sec.

Superficial liquid velocity (V_L) = 9.08 ft/sec.

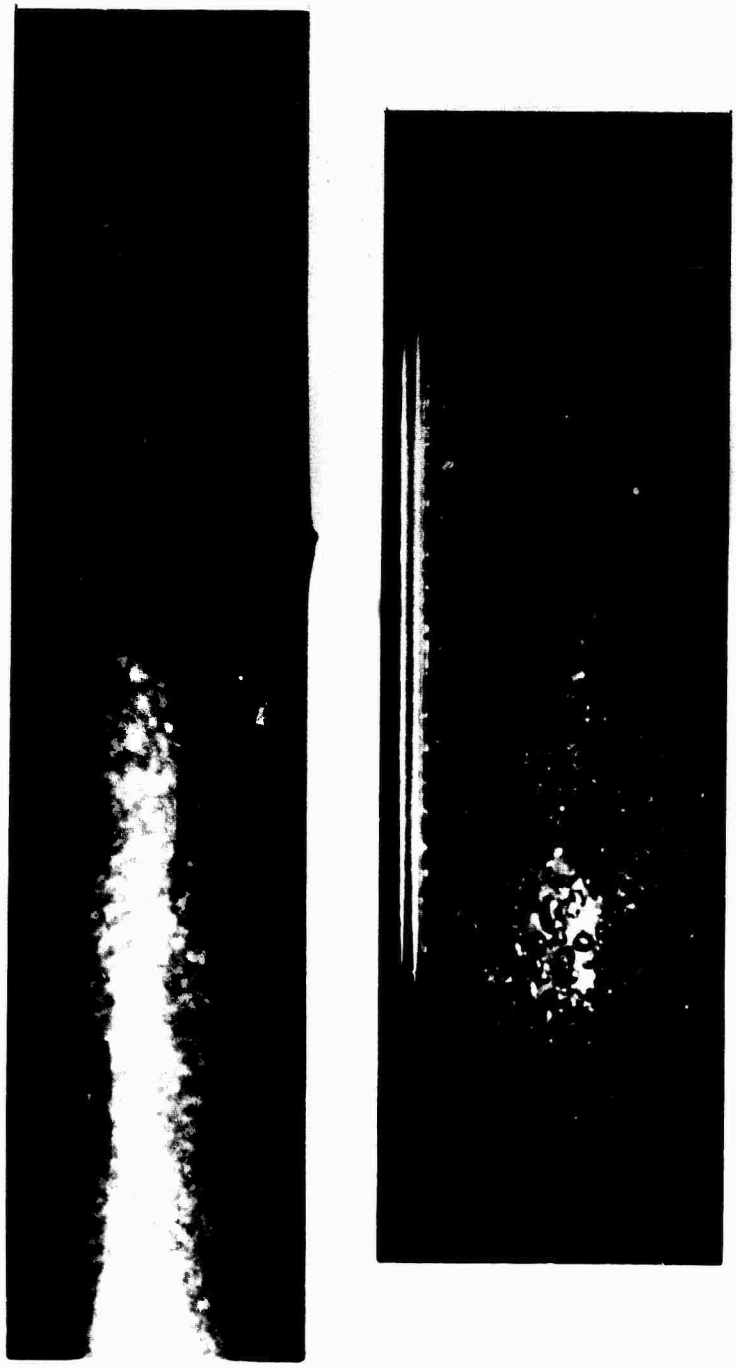

X-ray Flash

AERE - M 2159 Fig. 11

Simultaneous X-ray and flash photographs of air-water flow showing evidence of developing structure.

Run No. 109

Pressure = 45.3 PSIG

Superficial gas velocity (V_G) = 5.11 ft/sec.

Superficial liquid velocity (V_L) = 6.74 ft/sec.

X-ray

Flash

AERE - M 2159 Fig. 12

Simultaneous X-ray and flash photographs of air-water flow in the churn regime.

Run No. 58

Pressure = 6.5 PSIG

Superficial gas velocity (V_G) = 5.85 ft/sec.

Superficial liquid velocity (V_L) = 0.25 ft/sec.

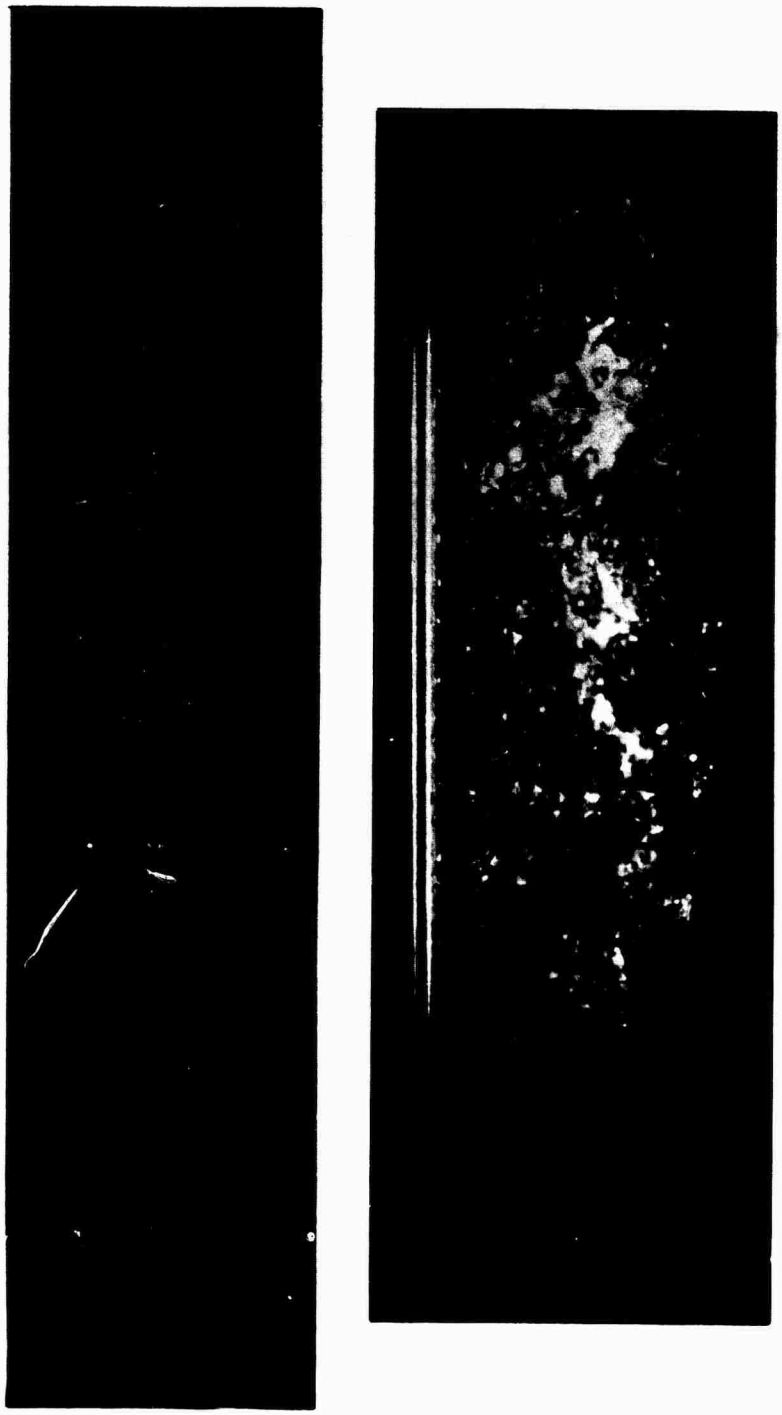

X-ray Flash

AERE - M 2159 Fig. 13

Simultaneous X-ray and flash photographs of air-water flow in the churn regime.

Run No. 101

Pressure = 45.3 PSIG

Superficial gas velocity (V_G) = 9.21 ft/sec.

Superficial liquid velocity (V_L) = 2.52 ft/sec.

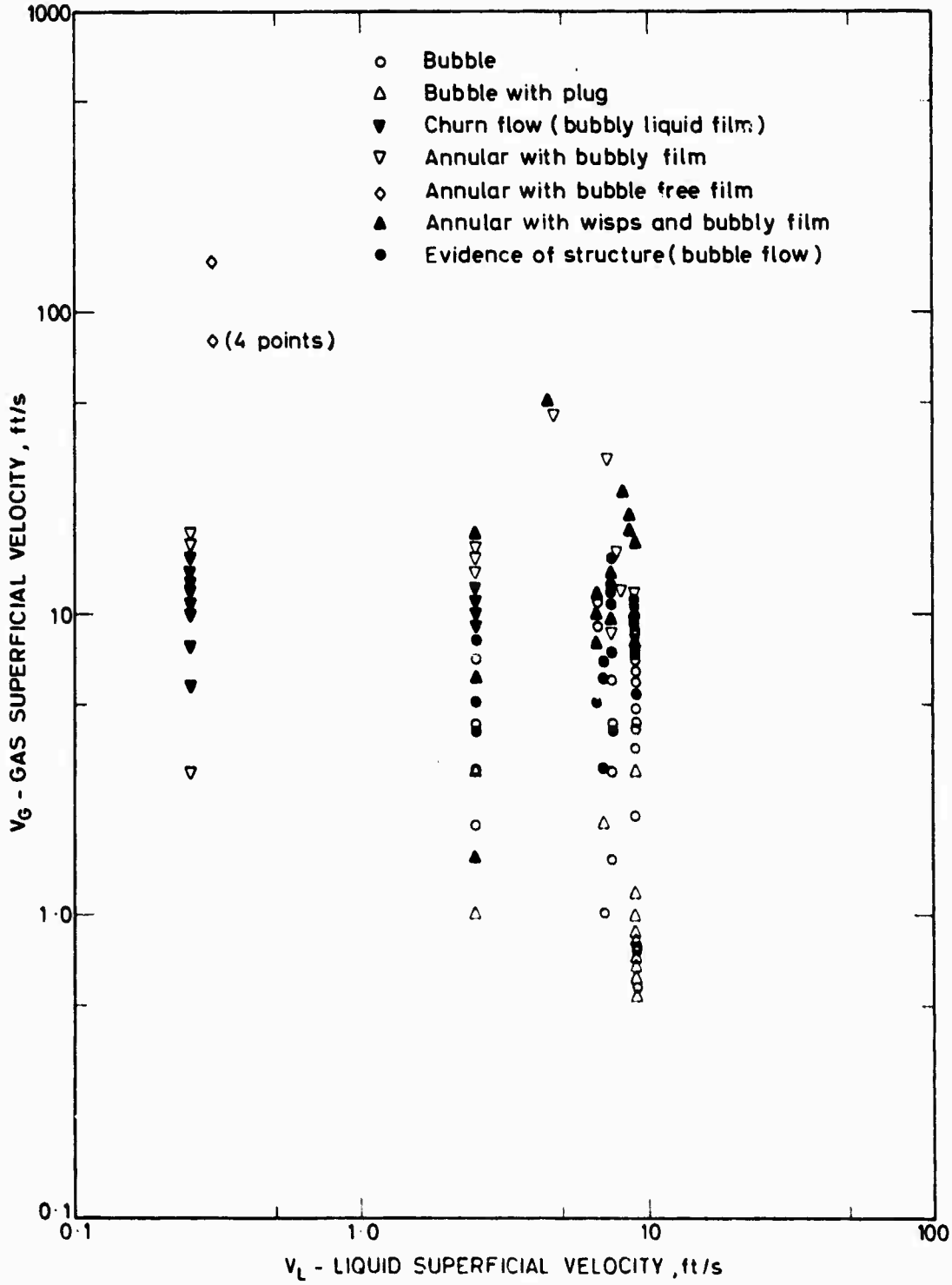

FLOW PATTERN MAP PLOTTED IN TERMS OF SUPERFICIAL VELOCITIES

FIGURE 14. A.E.R.E. M.2159

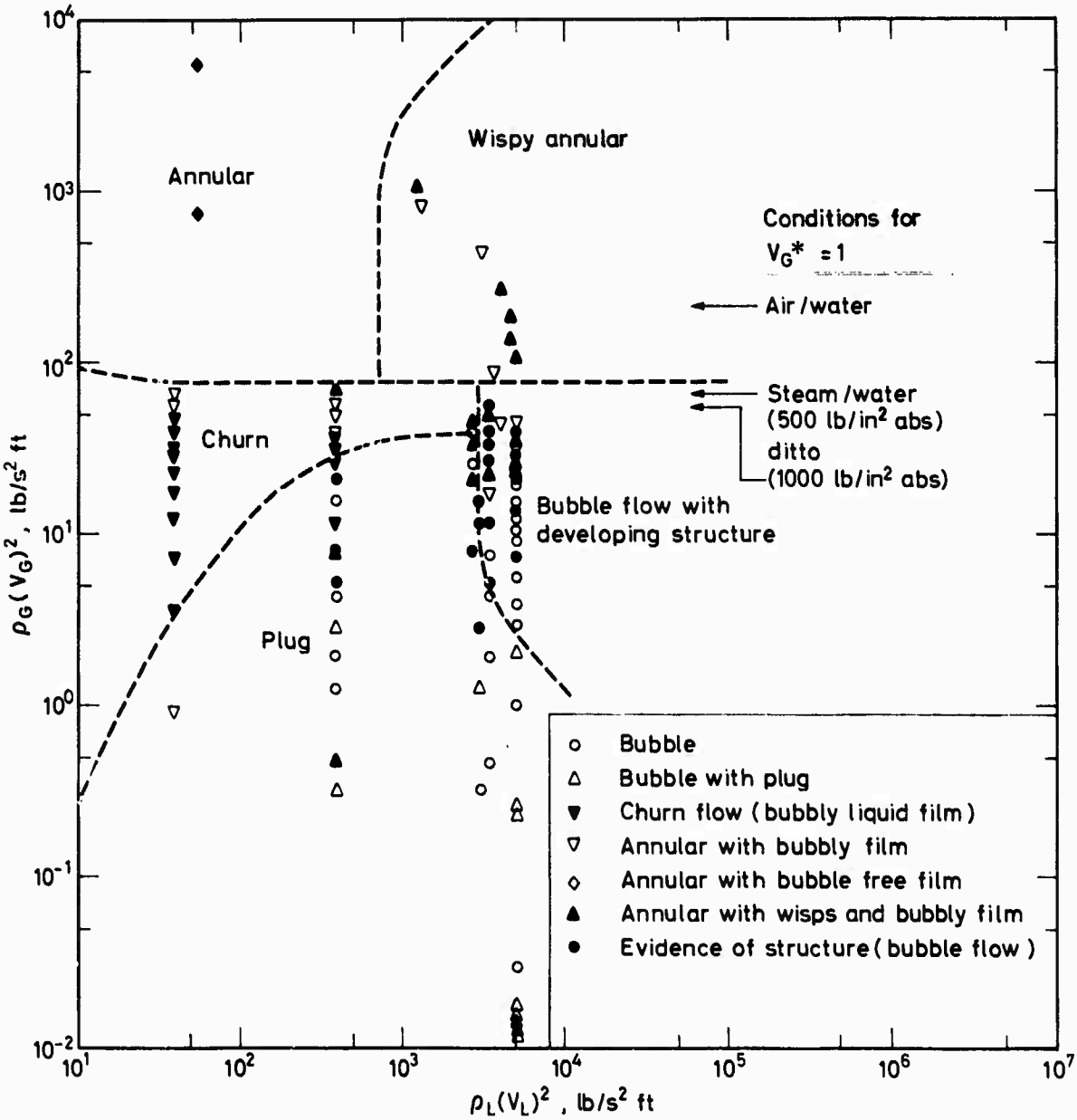

FLOW PATTERN MAP PLOTTED FROM DATA IN TABLE 1.

FIGURE 15. A.E.R.E. M.2159

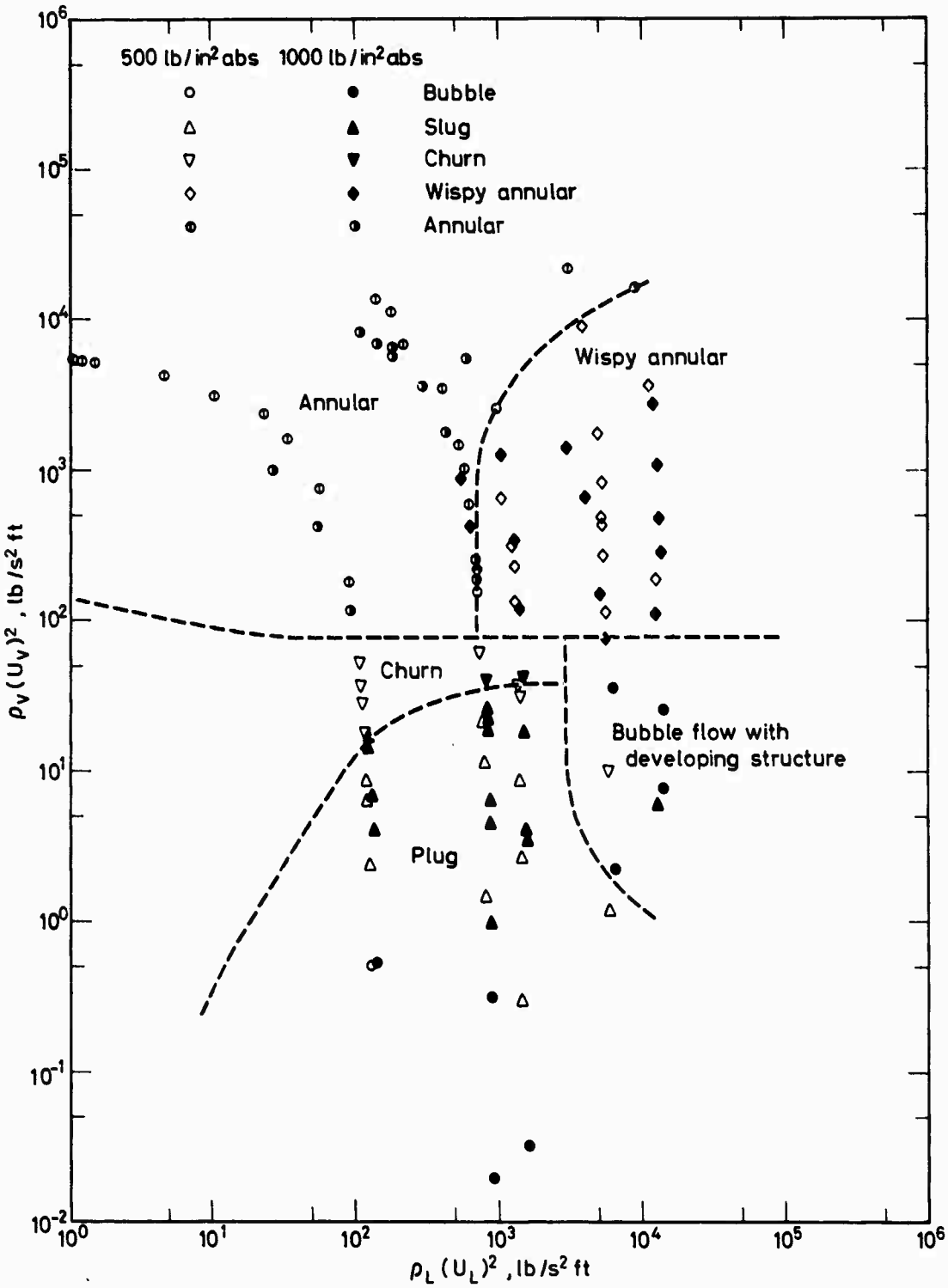

FLOW PATTERN MAP PLOTTED FROM RESULTS OBTAINED BY BENNETT et al.[5]

FIGURE 16. A.E.R.E. M.2159